



Virtual calibration of a supply air temperature sensor in rooftop air conditioning units

Daihong Yu , Haorong Li , Yuebin Yu & Jun Xiong

To cite this article: Daihong Yu , Haorong Li , Yuebin Yu & Jun Xiong (2011) Virtual calibration of a supply air temperature sensor in rooftop air conditioning units, HVAC&R Research, 17:1, 31-50

To link to this article: <https://doi.org/10.1080/10789669.2011.543250>



Published online: 18 Feb 2011.



Submit your article to this journal [↗](#)



Article views: 131



View related articles [↗](#)



Citing articles: 10 View citing articles [↗](#)

Virtual calibration of a supply air temperature sensor in rooftop air conditioning units

Daihong Yu,^{1,*} Haorong Li,¹ Yuebin Yu,² and Jun Xiong¹

¹Department of Architectural Engineering, University of Nebraska-Lincoln, Omaha, NE, USA

²Center for Building Performance and Diagnostics, Carnegie Mellon University, Pittsburgh, PA, USA

*Corresponding author e-mail: daisy.yu926@gmail.com

Supply air temperature (SAT) measurement is an important element in sequencing control and automated fault detection and diagnosis (AFDD) in HVAC systems to ensure the comfort of building occupants, decrease energy consumption, and lower maintenance cost. But in rooftop air conditioning units (RTUs) with gas-fired heating, the accuracy and reliability of manufacturer-installed supply air temperature (MSAT) sensors are notoriously difficult to attain. Experimental evaluations in this study, covering both the cooling and heating modes and using both direct measurements of a MSAT sensor and a multi-sensor measuring grid, demonstrate that direct measurements cannot obtain the true value of SAT in RTUs in the heating mode. Erratic measurement errors exist due to nonuniform temperature distribution and intensive thermal radiation in a compact chamber. An innovative indirect virtual calibration method for an MSAT sensor is proposed in this article to solve this issue. It demonstrates that a virtual calibrated MSAT sensor can provide accurate results when combined with a linear correlation for offset error that depends on heating stage and outside air damper signals. The linear correlation could be determined using the calculated temperature difference between the predicted theoretical true value of SAT and the direct MSAT measurement. This virtual calibration method is generic for all RTUs with similar construction of gas furnaces and can be implemented for long-term use. Further experimental evaluation and uncertainty analysis prove that the virtual calibration method can accurately predict the true value of SAT in RTUs within $\pm 1.2^\circ\text{F}$ (0.7°C) uncertainty. This economical technology will not only improve energy management of packaged units in sequencing control but also better facilitate real-time automated control and fault detection and diagnosis.

Introduction

Approximately half of all U.S. commercial floor space is conditioned by self-contained, packaged air-conditioning units, mostly located on the roof. Commercial rooftop air-conditioning units (RTUs) configured with cooling/heating equipment and air-handling fans are available ranging from 1 ton to

more than 100 tons of air-conditioning capacity. The U.S. Department of Energy (DOE) estimates that RTUs including unitary air-conditioning equipment account for about 1.66 quads of total energy consumption for commercial buildings in the United States (Westphalen and Koszalinski 2001). Badly maintained, degraded, and improperly controlled equipment wastes about 15% to 30% of

Received February 3, 2010; accepted July 20, 2010

Diahong Yu is a PhD student and Student Member ASHRAE. **Haorong Li, PhD**, is assistant professor and Member ASHRAE.

Yuebin Yu is PhD student. **Jun Xiong, PhD**, is a post doctor.

energy used in commercial buildings (Katipamula and Brambley 2005). As a key component, the supply air temperature (SAT) sensor is widely installed in light commercial RTUs and plays a significant role in sequencing controls and performing automated fault detection and diagnosis (AFDD).

According to the manufacturers' technical publication (Lennox 2007), discharge (supply) air control of heating (DACH) stages or discharge (supply) air control of cooling (DACC) stages can be enabled when a zone sensor module or a local thermostat calls for heating or cooling so that the RTU performance can be improved in the following perspectives:

- better humidity control with the SAT stabilized at 55°F (12.8°C) (default DACC set-point is 55°F [12.8°C]);
- energy savings through economizer control by adjusting the free cooling set-point approximately 2°F (1.1°C) lower than the DACC set-point;
- energy savings by embedding both outside air temperature (OAT) reset and return air temperature (RAT) reset to adjust the DACH and DACC set-points; for example, in the mode of DACH, the OAT reset saves energy by gradually decreasing the DACH set-point as the OAT increases.

AFDD aimed at early identification and isolation of premature faults trends to be an emerging technology in the field of HVAC. Over the last decade, a number of research funded by the DOE, ASHRAE, and other institutions has been completed or undertaken to utilize AFDD to improve RTUs' performances (e.g., Rossi 1995; Rossi and Braun 1997; Breuker 1997; Breuker and Braun 1998a, 1998b; Li and Braun 2003, 2007a, 2007b, 2007c).

The SAT measurement is a critical element in the use of AFDD technology for performance monitoring, controlling, diagnostics, and optimization of packaged air-conditioning units. It is typically used as an input in determining supply air fan temperature rise, mixed air temperature (MAT), supply air humidity ratio, and temperature difference across cooling or heating coil. These quantities are used for system monitoring and within diagnostic algorithms (Rossi and Braun 1997; Li and Braun 2003, 2007b, 2007c; Wichman and Braun 2009). They can also be used in combination with compressor maps to predict sensible cooling capacity (Li and Braun 2007c) for performance fault diagnostics and impact evaluation, and they can be used to derive de-

coupling features (Li and Braun 2007b, 2007c) that provide an indication of fault levels (fault severity).

In summary, a manufacturer-installed supply air temperature (MSAT) sensor is widely used in most light commercial RTUs, and it plays an important role in improving the sequencing control and enabling AFDD technology in RTUs. However, as described in the following section, there are many challenges associated with the use of MSATs in RTUs for the above two applications.

A common practice by RTU manufacturers is to pre-install the MSAT sensor right after the gas-fired heating coil in a compact chamber. Owing to the following two inherent problems under this arrangement, the accuracy and reliability of the MSAT sensor are notoriously difficult to attain in heating mode (ASHRAE 2009):

- *Poor air temperature distribution:* With a gas-fired heating coil mounted in a crowded housing, RTUs have an extremely uneven air temperature distribution where the onboard SAT sensor is located. According to ASME PTC 19.3-1974, the aspiration method involving passing a high-velocity stream of air over the temperature sensor is improbable to be applied.
- *Intensive thermal radiation of gas heating:* The MSAT sensor is bathed in an adverse hot-air chamber. Measurements can be affected by radiation from surrounding surfaces (ASHRAE 2009). Strong thermal radiation from gas burners causes a dramatic rise in air temperature measurement. Even with the shielding suggested by Parmelee and Huebscher (1946), the radiation impact on the MSAT sensor can hardly be eliminated. Meanwhile, the RTU's compact structure makes it improper for shielding.

Consequently, manufacturers recommend that the MSAT sensor should be relocated to the supply air duct on site if the discharge air control functions were used (Lennox 2007). However, relocating the MSAT sensor would initiate a series of problems.

First of all, repositioning the MSAT sensor to the supply air duct could be very costly in a situation where all other installations of a system are completed. It is greatly in excess of the original budget planned for an economy packaged unit. Second, RTUs are usually set up right upon the roof of the served zones in light commercial buildings (e.g., big-box retail stores); the supply air duct, if there is one, is too short to meet the minimum

requirements by manufacturers or to achieve a balanced air temperature distribution.

As a result, many building operators either do not bother to relocate the MSAT sensor, which will cause unreliable discharge air control, or completely disable the MSAT sensor and the discharge air control function.

No research so far has provided a proper solution to address the above issues. Instead of repositioning the MSAT sensor to the supply air duct or directly using the MSAT measurements, this article proposes an innovative virtual calibration method to solve the dilemma. The main merit of this method is that a general linear model to offset the MSAT errors is created through a one-time algorithm development. This virtual calibration technique is very cost effective, accurate, stable, easy to use, and generic for all RTUs with similarly constructed of gas furnaces, and it can be implemented for long-term use. It is a very promising approach that could significantly improve the cost effectiveness and energy management through DACH or DACC in RTUs as well as enabling and insuring better performance of AFDD applications.

The study begins with the evaluation of two groups of direct measurements: the single onboard MSAT-sensor-based measurement and a measuring-grid-based measurement. It is found that neither method can provide the real-time true value of the SAT. There are unstable changing errors in both of them, which rules out the possibility of using regular calibration. Then, a virtual calibration algorithm for the MSAT sensor is proposed based on lab data, and also the modeling and implementation procedures are summarized for easy-to-use implementation. Uncertainty analysis and additional experimental evaluation are carried out over a wide range of controlled tests later on. The study concludes that the virtual calibration technology can accurately predict the real-time measuring offset and the true value of the SAT in RTUs.

Evaluation of direct measurements

Direct measurements are conventionally used for air temperature in all kinds of forced-air systems. In this section, an RTU equipped with gas heating is evaluated in terms of direct SAT measuring with two

methods: the MSAT-sensor-based measurement and a measuring-grid-based measurement.

The assessment starts with the single onboard MSAT sensor under both cooling and heating modes. To further understand the nature of inaccuracy in direct measurement, an additional method, termed the multi-sensor measuring grid, is applied. The measurements are performed simultaneously in the same experimental series to ensure the consistency and comparability of the results. To keep it simple, only the necessary experimental results and the deduction are debriefed in what follows. Detailed experimental settings and considerations are elaborated in the Appendix, Part A.

MSAT-sensor-based measurement

A group of parametric tests are implemented to a two-stage cooling and two-stage gas-heating RTU for the evaluation of the MSAT-sensor-derived measurements. Both cooling and heating modes are offered with stage 1 and 2. Outside air damper position (OADst) is modulated at 0% and 30% for the different runs, since in cooling and heating modes, RTUs bring in minimum outside air flow for ventilation, and 30% is usually the upper limit for a minimum damper position (ASHRAE 2007).

In Table 1, experiment settings and results are provided. The error e accounts for the difference between the average measurements of the MSAT sensor ($SAT_{mfr,meas}$) and the additional lab-installed SAT sensor ($SAT_{lab,meas}$):

$$e = SAT_{lab,meas} - SAT_{mfr,meas}. \quad (1)$$

It can be seen from the results that

- in the cooling mode, the direct measurements are considered reliable with e less than 2.0°F (1.1°C);
- however, in the heating mode, direct measurements with both sensors lose credibility since e widely varies from 21.0°F (11.7°C) to 34.6°F (19.2°C).

Therefore, further analysis to evaluate the MSAT-sensor-based measurement in the heating mode is carried out by comparing $SAT_{mfr,meas}$ to the predicted theoretical true value of the SAT ($SAT_{th,pred}$) as e_H :

$$e_H = SAT_{mfr,meas} - SAT_{th,pred}, \quad (2)$$

Table 1. Evaluation of MSAT sensor-based measurement under both cooling and heating modes.

Running mode	Running stage	Scenario		$SAT_{lab,meas}$ ($^{\circ}\text{F}$ ($^{\circ}\text{C}$))	$SAT_{mfr,meas}$ ($^{\circ}\text{F}$ ($^{\circ}\text{C}$))	$SAT_{mfr,meas}$ ($^{\circ}\text{F}$ ($^{\circ}\text{C}$))	e ($^{\circ}\text{F}$ ($^{\circ}\text{C}$))			
		OADst	ID							
Cooling	2	0%	C-1	48.2 (9.0)	46.2 (7.9)	2.02 (1.1)				
Cooling	2	0%	C-2	38.8 (3.8)	36.8 (2.7)	2.0 (1.1)				
Cooling	2	30%	C-3	51.2 (10.7)	49.4 (9.7)	1.8 (1.0)				
Cooling	2	30%	C-4	50.4 (10.2)	48.4 (9.1)	1.9 (1.1)				
Cooling	1	0%	C-5	62.3 (16.8)	61.3 (16.3)	1.0 (0.6)				
Cooling	1	0%	C-6	56.4 (13.6)	55.8 (13.2)	0.5 (0.3)				
Cooling	1	30%	C-7	66.4 (19.1)	65.9 (18.8)	0.5 (0.3)				
Cooling	1	30%	C-8	66.0 (18.9)	64.6 (18.1)	1.4 (0.8)				
Running mode	Running stage	OADst	Scenario ID	$SAT_{lab,meas}$ ($^{\circ}\text{F}$ ($^{\circ}\text{C}$))	$SAT_{mfr,meas}$ ($^{\circ}\text{F}$ ($^{\circ}\text{C}$))	\dot{V}_{meas} (cfm (m^3/s))	$SAT_{th,pred}$ ($^{\circ}\text{F}$ ($^{\circ}\text{C}$))	MAT ($^{\circ}\text{F}$ ($^{\circ}\text{C}$))	e_H ($^{\circ}\text{F}$ ($^{\circ}\text{C}$))	e ($^{\circ}\text{F}$ ($^{\circ}\text{C}$))
Heating	2	0%	H-1	151.4 (66.3)	120.1 (48.9)	1848 (0.87)	108.0 (42.2)	54.2 (12.3)	12.1 (6.7)	31.3 (17.4)
Heating	2	0%	H-2	151.3 (66.3)	120.0 (48.9)	2045 (0.97)	108.3 (42.4)	59.5 (15.3)	11.7 (6.5)	31.3 (17.4)
Heating	2	0%	H-3	152.5 (66.9)	121.5 (49.7)	1857 (0.88)	108.9 (42.7)	55.4 (13.0)	12.6 (7.0)	31.0 (17.2)
Heating	2	0%	H-4	155.1 (68.4)	124.0 (51.1)	1829 (0.86)	111.8 (44.3)	57.4 (14.1)	12.2 (6.8)	31.1 (17.3)
Heating	2	30%	H-5	134.4 (56.9)	99.9 (37.7)	2076 (0.98)	93.0 (33.9)	44.9 (7.2)	6.9 (3.8)	34.5 (19.2)
Heating	2	30%	H-6	138.5 (59.2)	104.5 (40.3)	2269 (1.07)	96.7 (35.9)	52.5 (11.4)	7.8 (4.3)	34.1 (18.9)
Heating	2	30%	H-7	140.5 (60.3)	106.1 (41.2)	2037 (0.96)	99.2 (37.3)	50.2 (10.1)	7.0 (3.9)	34.4 (19.1)
Heating	2	30%	H-8	144.4 (62.4)	109.9 (43.3)	2040 (0.96)	102.7 (39.3)	53.8 (12.1)	7.2 (4.0)	34.6 (19.2)
Heating	1	0%	H-9	120.4 (49.1)	99.4 (37.4)	1853 (0.87)	94.7 (34.8)	59.3 (15.2)	4.6 (2.6)	21.1 (11.7)
Heating	1	0%	H-10	119.1 (48.4)	98.1 (36.7)	2051 (0.97)	93.2 (34.0)	61.0 (16.1)	4.9 (2.7)	21.0 (11.7)
Heating	1	0%	H-11	122.1 (50.1)	100.8 (38.2)	1849 (0.87)	96.4 (35.8)	60.9 (16.1)	4.3 (2.4)	21.4 (11.9)
Heating	1	0%	H-12	124.1 (51.2)	102.6 (39.2)	1831 (0.86)	99.6 (37.6)	63.7 (17.6)	3.0 (1.7)	21.4 (11.9)
Heating	1	30%	H-13	106.1 (41.2)	82.6 (28.1)	2081 (0.98)	80.4 (26.9)	48.6 (9.2)	2.2 (1.2)	23.5 (13.1)
Heating	1	30%	H-14	106.4 (41.3)	83.2 (28.4)	2272 (1.07)	82.1 (27.8)	52.9 (11.6)	1.0 (0.6)	23.3 (12.9)
Heating	1	30%	H-15	111.0 (43.9)	87.5 (38.3)	2059 (0.97)	85.5 (29.7)	53.4 (11.9)	2.0 (1.1)	23.5 (13.1)
Heating	1	30%	H-16	114.8 (46.0)	90.8 (32.7)	2046 (0.97)	88.7 (31.5)	56.4 (13.6)	2.1 (1.2)	24.0 (13.3)

where $SAT_{th,pred}$ is derived from an energy balance, shown as Equation 3:

$$SAT_{th,pred} = \frac{\dot{Q}_H}{C_P \times \dot{V}_{meas}} v + MAT + \Delta T_{fan}, \quad (3)$$

where \dot{Q}_H is the heating capacity in Btu/hr (kJ/s), \dot{V}_{meas} is the measured supply air flow rate in cfm (m^3/s), C_P is the specific heat at constant pressure in Btu/(lbm $^\circ$ F) (kJ/(kg \cdot K)), v is the specific volume of air in lb/ft 3 (m^3/kg), MAT is the MAT before the gas burner in $^\circ$ F ($^\circ$ C), and ΔT_{fan} is the supply fan temperature rise in $^\circ$ F ($^\circ$ C).

The procedures of measuring the parameters in Equations 1–3 are addressed in detail in the Appendix, Part A. As given in Table 1, e_H is found to be unstable with the MSAT-sensor-based measurement. It alters in a wide range from 1.0 $^\circ$ F (0.6 $^\circ$ C) to 12.6 $^\circ$ F (7.0 $^\circ$ C) when test condition varies. It is obviously improper to directly use $SAT_{mfr,meas}$ in the heating mode as the true value of the SAT in the RTU. The results also demonstrate that a regular calibration with a fixed offset based on the MSAT-sensor-based direct measurement would fail.

Measuring-grid-based measurement

A measuring grid in the inlet of the supply air duct and right out of the RTU is also constructed for the experiments. Since the grid is not located in the chamber, the radiation influence from the gas burner can be attenuated to some extent. The multi-point measurements employed in a measuring grid are also supposed to improve the overall measurement accuracy with less stratification impact. Eight temperature sensors are positioned in the duct work after the RTU, as depicted in Figure 1. With eight sensors, the duct section representative locations are well covered.

Average values of each sensor from 1 to 8 ($SAT_{G,C}$ for the cooling mode and $SAT_{G,H}$ for the heating mode); the MSAT-sensor-based $SAT_{mfr,meas}$ and the calculated $SAT_{th,pred}$ are plotted in Figure 2 for comparison. The horizontal axis is for different sensor ID, and the vertical axis is for air temperatures in Fahrenheit and Celsius degrees. To get a clear view, the results of all cooling scenarios and half of the 16 heating scenarios are given in Figure 2.

The results of the cooling mode illustrate that the measurements of eight $SAT_{G,C}$ are close to those of $SAT_{mfr,meas}$. In all cooling scenarios, the error be-

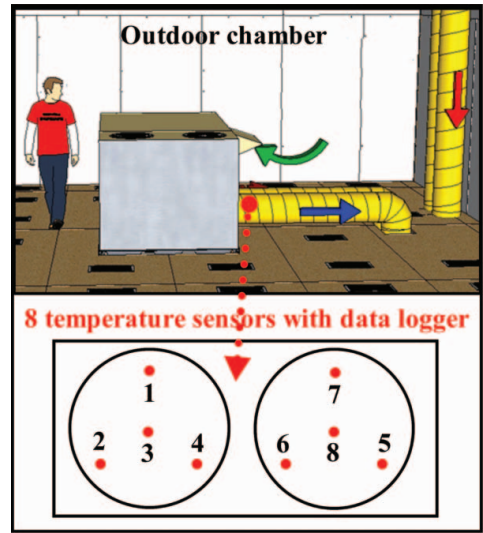


Figure 1. Illustration of measuring grid and numbered sensors.

tween the mean of eight $SAT_{G,C}$ and $SAT_{mfr,meas}$ is about 1.5 $^\circ$ F (0.8 $^\circ$ C) or less. It is consistent with the previous evaluation for the MSAT-sensor-based direct measurement. Both the MSAT sensor and the measuring grid in the cooling mode are trustworthy for use.

From the heating mode plot, the following points can be observed:

- Temperature distribution of eight $SAT_{G,H}$ is irregular: Combining Figures 1 and 2, the relationships of eight $SAT_{G,H}$ and their location in the heating mode are erratic. Temperature values of sensors 1 to 4 are lower than those of the corresponding sensors 5 to 8. It is unsuitable to calculate the true value of the SAT by averaging eight $SAT_{G,H}$.
- A big temperature difference exists between $SAT_{mfr,meas}$ and the average eight $SAT_{G,H}$: In scenario H-7, for example, $SAT_{mfr,meas}$ is 106.1 $^\circ$ F (41.2 $^\circ$ C); $SAT_{G,H}$ sensors 1 to 8 give the lowest reading as 74.4 $^\circ$ F (23.6 $^\circ$ C) and the highest as 108.7 $^\circ$ F (42.6 $^\circ$ C). It makes the differential temperature between $SAT_{mfr,meas}$ and the average eight $SAT_{G,H}$ 8.9 $^\circ$ F (4.9 $^\circ$ C). In all heating scenarios, the error between $SAT_{mfr,meas}$ and the mean of eight $SAT_{G,H}$ varies from 3.0 $^\circ$ F (1.7 $^\circ$ C) to 12.2 $^\circ$ F (6.8 $^\circ$ C).
- Various temperature difference stands between $SAT_{th,pred}$ and the mean of eight $SAT_{G,H}$: The temperature difference between $SAT_{th,pred}$ and the mean of eight $SAT_{G,H}$ varies in different scenarios. For example, in scenario H-7, with

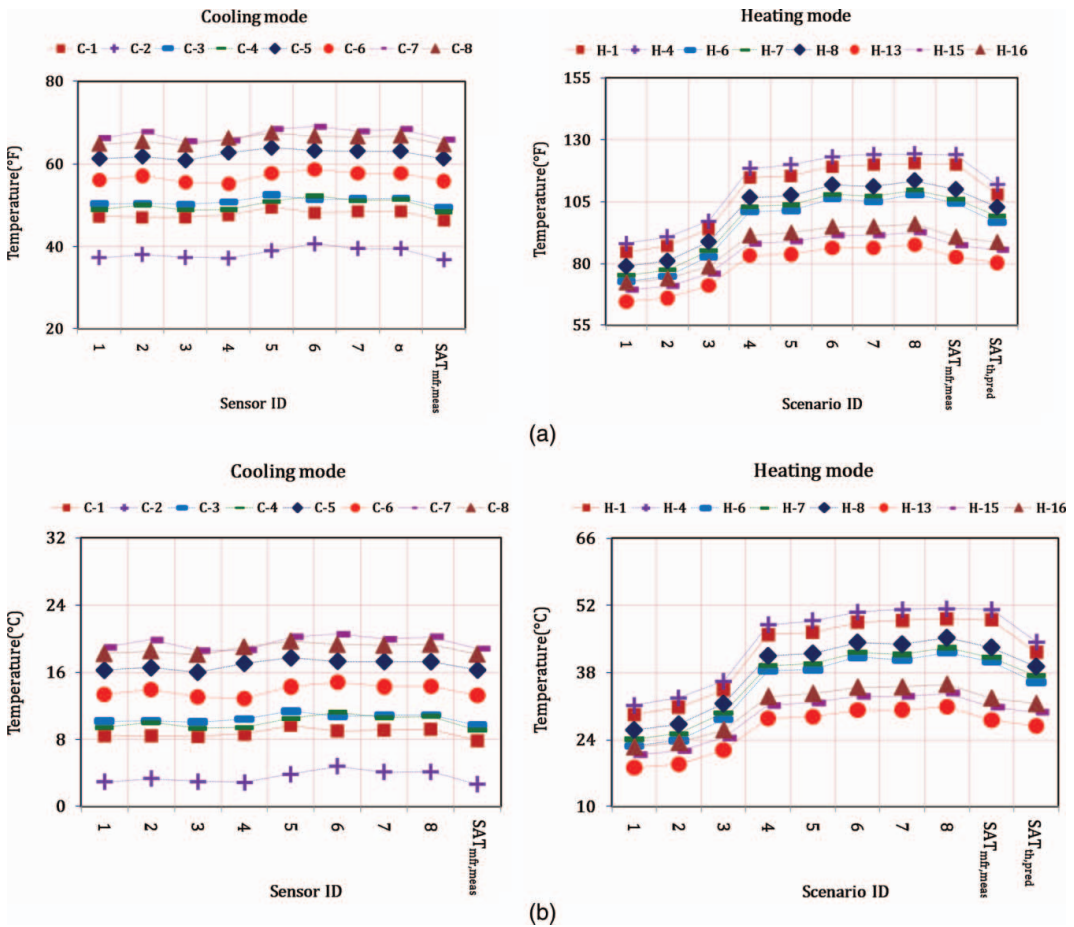


Figure 2. Evaluation of measuring grid under both cooling and heating modes: (a) IP units and (b) SI units.

heating stage (Hstage) 2 and OADst 30%, the mean of eight $SAT_{G,H}$ is 95.2°F (35.1°C) while the true value $SAT_{th,pred}$ is 99.2°F (37.3°C) (with 4.0°F [2.2°C] temperature difference). However, in scenario H-16 with Hstage 1 and OADst 30%, the mean of eight $SAT_{G,H}$ is 85.9°F (29.9°C) while the true value $SAT_{th,pred}$ is 88.7°F (31.5°C) (with 2.8°F [1.6°C] temperature difference). As presented in this case, the measuring grid does not indicate the true value of the SAT.

In summary, the evaluation of the measuring grid further testifies that the offset error for the MSAT in heating mode varies. Controls in RTUs related to MSAT sensor direct measurements in the heating mode can be far from the intended operation and lead to inferior system performance. In addition, using the measuring grid does not help obtain the true value of the SAT in RTUs. It also could not be

used for the verification of the predicted true value of the SAT. An innovative calibration algorithm is needed to fill in the gap.

Algorithm development and implementation issues

Algorithm development

As analyzed above, direct measurement, either the single MSAT-sensor-based or the measuring-grid-based, cannot catch the true value of the SAT. The measuring-grid method in a location out of the RTU merely provides a closer but still mediocre prediction. Besides, additional construction, costs, maintenance, and sources for uncertainty are incurred by using the measuring grid. It is not a practical tool in real applications.

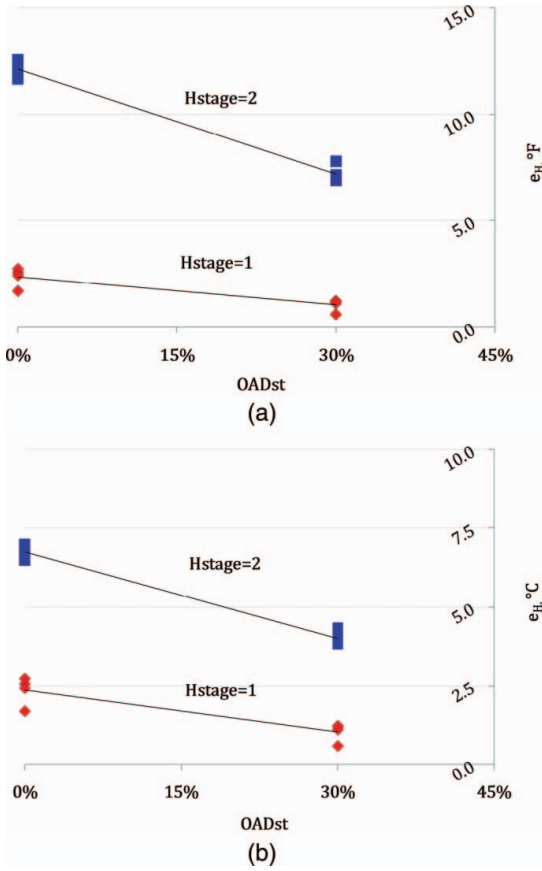


Figure 3. e_H vs OADst in different Hstage: (a) IP units and (b) SI units.

Variables in the experiments are thus reinvestigated to identify the algorithm that might be useful to predict the offset for the calibration of the MSAT-sensor-based measurement.

As shown in Figure 3, error e_H is a strong function of Hstage and OADst. A linear model can be fitted to represent the relationship between e_H , Hstage, and OADst in RTUs. As shown in Equation 4, the model can be used to estimate the calibration error (e_{cal}) of the MSAT sensor under certain Hstage and OADst; verification through more lab tests is explored in later sections:

$$e_{cal} = a + b \times Hstage + c \times Hstage^2 + d \times OADst + f \times OADst^2 + g \times Hstage \times OADst. \quad (4)$$

Once such an offset e_{cal} expression is obtained for a given type of RTU, it can be utilized to correct the

MSAT-sensor-based measurement for the true value in RTUs. The equation for the calibrated MSAT sensor ($SAT_{mfr,cal}$) is given below:

$$SAT_{mfr,cal} = SAT_{mfr,meas} - e_{cal}. \quad (5)$$

For this 7.5-ton rooftop unit with 130,000 Btu/hr (38.1 kW) gas heating capacity, the coefficients for the linear model are obtained with the experimental data. The results are listed in Table 2, with R -square 0.98.

Equations 4 and 5 jointly constitute the model of the virtual calibration that can be directly transplanted to different RTUs.

Implementation issues

With the analysis of SAT direct measurements and algorithm development of the virtual calibration for an MSAT sensor presented above, a summary of implementation issues, including the procedures of a one-time model development and its implementation for long-term use in RTUs, can be given, as illustrated in Figure 4.

- **One-time development:** According to Equations 2 and 3, the measurements and inputs for the procedure of algorithm development are $SAT_{mfr,meas}$, \dot{Q}_H , \dot{V}_{meas} , MAT, and ΔT_{fan} . $SAT_{mfr,meas}$ is the measurement of an MSAT sensor. \dot{Q}_H can be referred to manufacturers' information. \dot{V}_{meas} can be obtained with the test and balance when the RTUs are installed at the beginning or measured through a one-time test. ΔT_{fan} can be calculated by using the way proposed by Wichman and Braun (2009). MAT is estimated using the approaches provided by Yang and Li (2010). The reader can refer to the Appendix, Part A, which explains these parameters in detail. The correlated virtual calibration model for the bias errors of an MSAT sensor is needed only once and generic for all RTUs with similar construction of gas furnaces.
- **Long-term use:** Once the one-time development is conducted, the implementation of virtual calibration for long-term use is ready and easy with the otherwise unpredictable errors under different operations. According to Equations 4 and 5, the measurements and inputs for long-term use are

Table 2. Linear model coefficients for the example RTU.

Coefficients		<i>a</i>	<i>b</i>	<i>c</i>	<i>d</i>	<i>f</i>	<i>g</i>
IP units	Value	1.0900	0.6905	2.4200	0.5484	0.1166	-8.5000
SI units	Value	0.6056	0.3836	1.3444	0.3047	0.0648	-4.7222

only Hstage, OADst, and $SAT_{mfr,meas}$, which are available in light commercial RTUs.

Uncertainty analysis

The virtual calibration algorithm of an MSAT sensor obtains $SAT_{mfr,cal}$ as the prediction of the SAT true value. In this section, the uncertainty sensitivity of $SAT_{mfr,cal}$ is studied for relative gas heating capacity, supply air flow rate, MAT, and supply fan temperature rise. The root sum square method of uncertainty calculation is applied to the variables. The random uncertainty is expressed in units °F (°C) as Equation 6:

$$\delta SAT_{mfr,cal} = \left[\left(\frac{\partial SAT_{mfr,cal}}{\partial \dot{Q}_H} \delta \dot{Q}_H \right)^2 + \left(\frac{\partial SAT_{mfr,cal}}{\partial \dot{V}_{meas}} \delta \dot{V}_{meas} \right)^2 + \left(\frac{\partial SAT_{mfr,cal}}{\partial MAT} \delta MAT \right)^2 + \left(\frac{\partial SAT_{mfr,cal}}{\partial \Delta T_{fan}} \delta \Delta T_{fan} \right)^2 \right]^{1/2}, \quad (6)$$

where $\delta \dot{Q}_H$, $\delta \dot{V}_{meas}$, δMAT , and $\delta \Delta T_{fan}$ are sensor uncertainties.

Table 3 summarizes the uncertainties of independent variables as inputs to Equation 6, as well as the calculated uncertainties of $SAT_{mfr,cal}$ as outputs. The detailed uncertainties of the inputs are given in the Appendix, Part A and Part C. As can be seen, the absolute uncertainty of the virtual calibrated SAT is lower than 1.2°F (0.7°C). It is in the range of acceptable error for temperature uncertainties in the HVAC industry.

The accuracy of the virtual calibrated MSAT ($SAT_{mfr,cal}$) in Equations 4 and 5 is further evaluated below by using the data from extensive experiments in this study.

Experimental evaluation of the SAT virtual calibration method

Evaluation is presented here to validate the accuracy of the virtual calibration model for its generalization in real projects. There is no direct way, but an indirect method is used to evaluate the accuracy of the virtual calibrated MSAT sensor in RTUs. This goal is achieved by carefully designing an

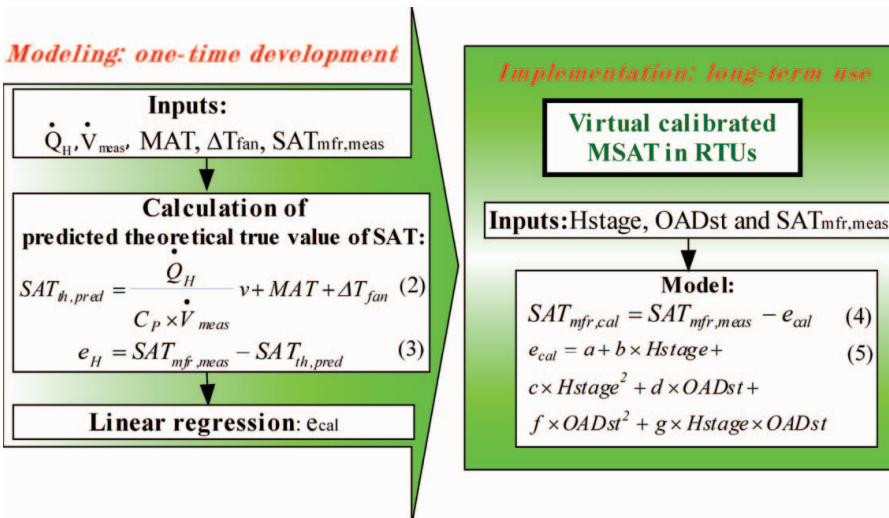
**Figure 4.** Modeling and implementation procedures for an MSAT sensor in RTUs.

Table 3. Uncertainty analysis of $SAT_{nff,cat}$.

Independent variables	Inputs	Uncertainty
Gas heating capacity, \dot{Q}_H (Btu/hr (kW))	Hstage 1: 84,500 (24.8) Hstage 2: 130,000 (38.1)	$\pm 2\%$
Measured supply air flow rate, \dot{V}_{meas} , (cfm (m ³ /s))	Default data in Table 1	$\pm 1\%$
MAT (°F (°C))	Default data in Table 1	$\pm 1.0^\circ\text{F}$ (0.6°C)
Supply fan temperature rise, ΔT_{fan} (°F (°C))	1.7°F (0.9°C)	$\pm 0.2^\circ\text{F}$ (0.1°C)
Dependent variable	Calibrated manufacturer-installed SAT sensor, $SAT_{nff,cat}$ (°F (°C))	
Scenario ID	H-1 H-2 H-3 H-4 H-5 H-6 H-7 H-8	
Uncertainty (°F)	1.2 (0.7) 1.1 (0.6) 1.2 (0.7) 1.2 (0.7) 1.1 (0.6) 1.1 (0.6) 1.1 (0.6) 1.1 (0.6)	1.1 (0.6) 1.1 (0.6) 1.1 (0.6) 1.1 (0.6) 1.1 (0.6) 1.1 (0.6) 1.1 (0.6) 1.1 (0.6)
Scenario ID	H-9 H-10 H-11 H-12 H-13 H-14 H-15 H-16	
Uncertainty (°F)	1.1 (0.6) 1.1 (0.6) 1.1 (0.6) 1.1 (0.6) 1.1 (0.6) 1.1 (0.6) 1.1 (0.6) 1.1 (0.6)	1.1 (0.6) 1.1 (0.6) 1.1 (0.6) 1.1 (0.6) 1.1 (0.6) 1.1 (0.6) 1.1 (0.6) 1.1 (0.6)

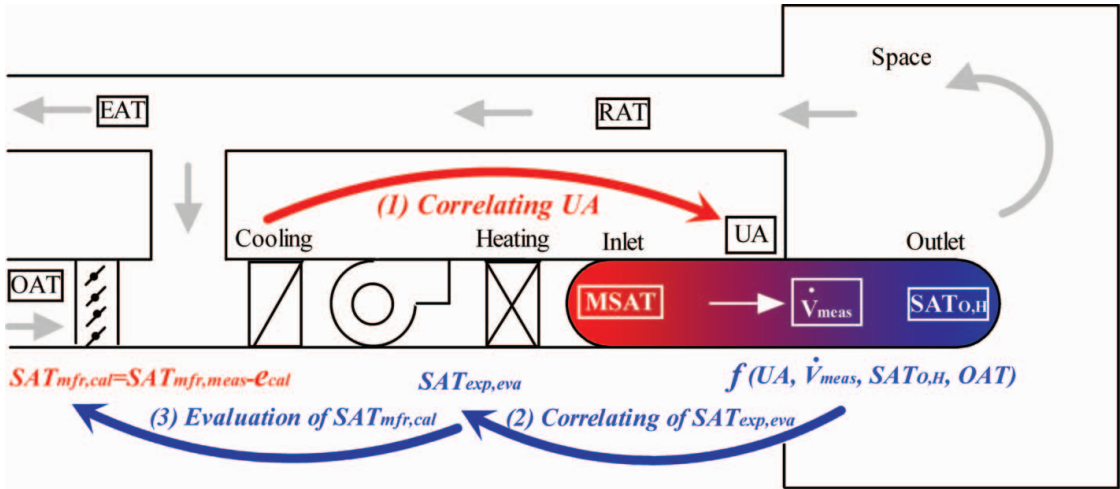


Figure 5. The experiment evaluation procedures of the virtual calibration methodology.

experiment in a laboratory environment. The detailed experiment configuration and analysis are given in the Appendix, Part A and Part B.

Evaluation layout

Figure 5 depicts the experiment evaluation procedures of the virtual calibration methodology presented in this article. The idea of using energy balance under both cooling (forward) and heating (backward) mode is innovatively conducted.

The verification is implemented by comparing $SAT_{mfr,cal}$ in Equation 4 to experimentally calculate the true value of SAT ($SAT_{exp,eva}$). $SAT_{exp,eva}$ is obtained based on an energy balance of the heat loss through the duct work. It is a counterpart of $SAT_{mfr,cal}$ but is used for evaluation purposes only. To calculate $SAT_{exp,eva}$, the knowns and assumptions are listed as follows:

- The mean of eight $SAT_{G,C}$ is regarded as the true value of the SAT in the cooling mode.
- Measurements of six air temperature sensors at the supply air duct outlet are reliable under both the heating ($SAT_{O,H}$) and cooling modes ($SAT_{O,C}$). The average of six $SAT_{O,H}$ and the average of six $SAT_{O,C}$ are used in the calculation. The supportive analysis of these temperatures is presented in the Appendix, Part B.
- UA of the supply air duct work from the measuring grid to the outlet is assumed to be constant under both cooling and heating modes.

- Supply air flow rate (\dot{V}_{meas}) and additional temperature measurements are taken in the location where the air is well mixed.

Evaluation implementation

Three main steps of evaluation in sequence are included as follows.

Step 1: Correcting UA in cooling mode. Heat loss in the cooling mode ($Q_{loss,C}$) through the duct work leads to the air temperature change from the measuring grid cross-section to the outlet in the duct. Heat transfer surface (A) and heat transfer coefficient (U) of the duct work are constants; therefore, UA could be deduced with \dot{V}_{meas} , OAT, $SAT_{G,C}$, and $SAT_{O,C}$.

Step 2: Correlating $SAT_{exp,eva}$. Similarly, $SAT_{exp,eva}$ in the heating mode should be acquired while UA, \dot{V}_{meas} , $SAT_{O,H}$, and OAT are known.

Step (3): Verification of $SAT_{mfr,cal}$

Finally, $SAT_{mfr,cal}$ in heating mode is evaluated after $SAT_{exp,eva}$ is derived from experiments.

Correcting UA in cooling mode

The goal here is to estimate the constant UA in the lab environment with the data points collected in the experiment series in cooling mode. To investigate the UA, it is assumed that (1) the overall heat transfer coefficient is constant, (2) the specific heat of air is constant, and (3) the supply air flow rate is constant because a fixed-fan speed is incorporated in the RTU.

Table 4. Correcting UA in cooling mode.

Scenario ID	\dot{V}_{meas} (cfm (m ³ /s))	$SAT_{O,C}$ (°F (°C))	$SAT_{G,C}$ (°F (°C))	OAT (°F (°C))	$Q_{loss,C}$ (Btu/hr(kW))	ΔT_C (°F (°C))
C-1	1931 (0.9)	49.4 (9.7)	48.0 (8.9)	81.8 (27.7)	2982 (0.87)	33.1 (18.4)
C-2	2328 (1.1)	41.1 (5.1)	38.6 (3.7)	87.8 (31.0)	6311 (1.85)	47.9 (26.6)
C-3	2084 (1.0)	52.3 (11.3)	51.1 (10.6)	82.3 (27.9)	2566 (0.75)	30.6 (17.0)
C-4	2595 (1.2)	51.9 (11.1)	50.3 (10.2)	87.0 (30.6)	4596 (1.35)	35.9 (19.9)
C-5	1874 (0.9)	63.0 (17.2)	62.5 (16.9)	79.6 (26.4)	1154 (0.34)	16.9 (9.4)
C-6	2251 (1.1)	58.5 (14.7)	57.0 (13.9)	81.8 (27.7)	3792 (1.11)	24.1 (13.4)
C-7	2026 (1.0)	66.5 (19.2)	66.0 (18.9)	81.9 (27.7)	1094 (0.32)	15.7 (8.7)
C-8	2526 (1.2)	68.2 (20.1)	67.4 (19.7)	86.4 (30.2)	2373 (0.70)	18.7 (10.3)

In the cooling mode, with \dot{V}_{meas} , OAT, $SAT_{G,C}$, and $SAT_{O,C}$ known, $Q_{loss,C}$ can be calculated:

$$Q_{loss,C} = \frac{\dot{V}_{meas} \times C_p \times (SAT_{O,C} - SAT_{G,C})}{v} \quad (7)$$

Meanwhile, $Q_{loss,C}$ also can be expressed as

$$Q_{loss,C} = UA \left(OAT - \frac{SAT_{O,C} + SAT_{G,C}}{2} \right) \quad (8)$$

Combining the two expressions gives

$$\frac{\dot{V}_{meas} \times C_p \times (SAT_{O,C} - SAT_{G,C})}{v} = UA \left(OAT - \frac{SAT_{O,C} + SAT_{G,C}}{2} \right) \quad (9)$$

Put variable ΔT_C as follows:

$$\Delta T_C = OAT - \frac{SAT_{O,C} + SAT_{G,C}}{2}$$

So, Equation 9 can be further simplified to the equation below:

$$Q_{loss,C} = UA \times \Delta T_C \quad (10)$$

Eight sets of \dot{V}_{meas} , OAT, $SAT_{G,C}$, and $SAT_{O,C}$, as well as the intermediate value $Q_{loss,C}$ and ΔT_C , are listed in Table 4.

Figure 6 shows that $Q_{loss,C}$ and ΔT_C have a positive linear correlation. Data points scatter closely beside a line. The slope of the linear-regressed line, which is 115.47, can be used as the value of UA for the duct work. In other words, UA is found as 115.47 Btu/hr °F (0.06 kW/K). As a physical

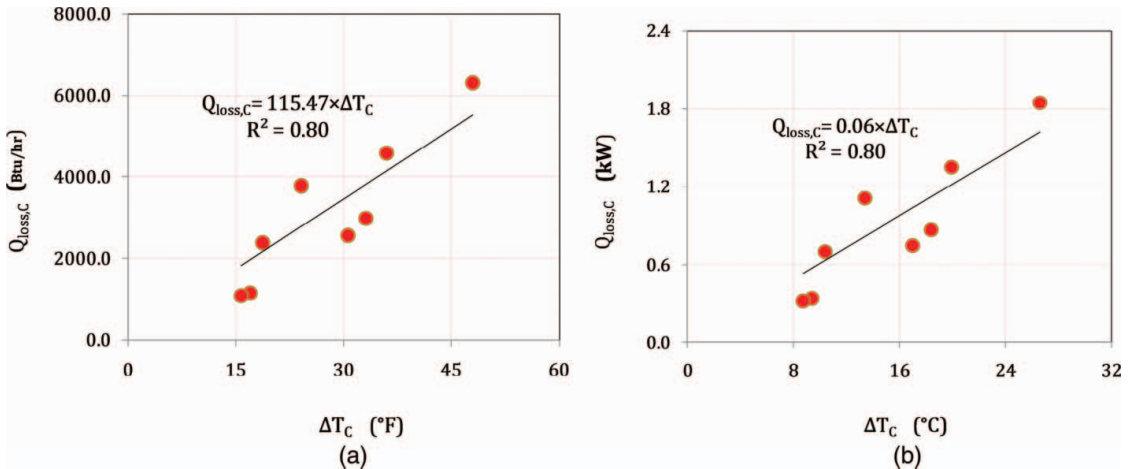
**Figure 6.** UA linear regression: (a) IP units and (b) SI units.

Table 5. Results of evaluation of $SAT_{mfr,cal}$.

Scenario ID	$SAT_{exp,eva}$ (°F (°C))	\dot{V}_{meas} (cfm (m ³ /s))	$SAT_{mfr,cal}$ (°F (°C))	e_{eva} (°F (°C))
H-1	108.6 (42.6)	1848 (0.87)	108.0 (42.2)	-0.6 (-0.3)
H-2	108.8 (42.7)	2045 (0.97)	108.3 (42.4)	-0.5 (-0.3)
H-3	110.1 (43.4)	1857 (0.88)	108.9 (42.7)	-1.1 (-0.6)
H-4	112.3 (44.6)	1829 (0.86)	111.8 (44.3)	-0.5 (-0.3)
H-5	92.4 (33.6)	2076 (0.98)	93.0 (33.9)	0.6 (0.3)
H-6	95.9 (35.5)	2269 (1.07)	96.7 (35.9)	0.7 (0.4)
H-7	98.4 (37.3)	2037 (0.96)	99.2 (37.3)	0.7 (0.4)
H-8	101.9 (39.3)	2040 (0.96)	102.7 (39.3)	0.8 (0.4)
H-9	95.2 (35.1)	1853 (0.87)	94.7 (34.8)	-0.5 (-0.3)
H-10	93.9 (34.4)	2051 (0.97)	93.2 (34.0)	-0.6 (-0.3)
H-11	96.7 (35.9)	1849 (0.87)	96.4 (35.8)	-0.3 (-0.2)
H-12	98.8 (37.1)	1831 (0.86)	99.6 (37.6)	0.8 (0.4)
H-13	80.8 (27.1)	2081 (0.98)	80.4 (26.9)	-0.4 (-0.2)
H-14	81.1 (27.3)	2272 (1.07)	82.1 (27.8)	1.0 (0.6)
H-15	85.5 (29.7)	2059 (0.97)	85.5 (29.7)	0.0 (0.0)
H-16	88.9 (31.6)	2046 (0.97)	88.7 (31.5)	-0.2 (-0.1)

characteristic of the duct work, this value remains unchanged when gas heating is operating.

Correlating $SAT_{exp,eva}$

As pointed out previously, with UA, \dot{V}_{meas} , $SAT_{O,H}$, and the OAT known, $SAT_{exp,eva}$ could be obtained by jointly solving Equations 11 and 12:

$$Q_{loss,H} = \frac{\dot{V}_{meas} \times C_p \times (SAT_{exp,eva} - SAT_{O,H})}{v}, \quad (11)$$

$$Q_{loss,H} = UA \left(OAT - \frac{SAT_{exp,eva} + SAT_{O,H}}{2} \right). \quad (12)$$

The results of $SAT_{exp,eva}$ are summarized in Table 5. From this point on, $SAT_{exp,eva}$ can be used to evaluate the accuracy of $SAT_{mfr,cal}$.

Evaluation of $SAT_{mfr,cal}$

To estimate the accuracy of $SAT_{mfr,cal}$, the error e_{eva} between $SAT_{mfr,cal}$ and $SAT_{exp,eva}$ given as Equation 13 is to be analyzed:

$$e_{eva} = SAT_{mfr,cal} - SAT_{exp,eva}. \quad (13)$$

The results are compiled in Table 5. The error e_{eva} is within the range of $\pm 1.1^\circ\text{F}$ (0.6°C). Thus,

$SAT_{mfr,cal}$ is demonstrated to be credible and can be trusted as the true value of the SAT in RTUs.

Conclusions and discussion

The single MSAT-sensor-based direct measurement is conventionally used in RTUs to obtain the SAT. But the accuracy and reliability is greatly compromised in the heating mode due to severe temperature stratification and high thermal radiation. The single onboard MSAT-sensor- and measuring-grid-based measurements are evaluated through a set of tests in a lab. The experiments are designed to cover representative operations in both cooling and heating modes. It is found that, although direct measurements have reasonably good accuracy in the cooling mode, there are unacceptable erratic errors in the heating mode and a regular calibration can hardly overcome the defect.

An easy-to-use virtual calibration methodology is then proposed. A general linear model relying on available operation information is derived to acquire the various offsets. Further, experimental evaluation and uncertainty analysis are conducted to prove the performance of this innovative method. The study indicates that the virtual calibration of an MSAT sensor in RTUs:

- is robust enough against various operating conditions,

- has very good accuracy (the uncertainty is $\pm 1.2^\circ\text{F}$ [0.7°C]),
- is easy to implement and economical for use, and
- is generic for all RTUs with similar construction of gas furnaces.

For SAT-based sequencing control in RTUs, improved energy efficiency and higher reliability could be achieved by using accurate measurements of a virtually calibrated MSAT sensor. Knowledge of the SAT true value in RTUs will also benefit real-time automated control, AFDD, and other advance applications. For instance,

- it could serve as part of a permanently installed control or monitoring system to ensure accuracy in SAT measurement;
- it could help find the Hstage failure fault in RTUs by evaluating the differential temperature across the gas furnaces; and
- it also could be utilized to develop a virtual supply airflow rate meter, which is important for monitoring, controlling, diagnosing, and optimizing indoor air quality and energy consumption in RTUs.

In this study, only RTUs with constant air volume (CAV) application are considered. However, variable air volume (VAV) becomes more and more popular in large commercial RTUs with a capacity larger than 30 tons. It is anticipated that the method could be adopted for VAV RTU systems used in larger commercial buildings. It could be a topic for future studies.

Nomenclature

A	= heat transfer area, ft^2 (m^2)
AFDD	= automated fault detection and diagnosis
C_a	= fluid capacity rate of air side, $\text{Btu}/(\text{hr}\cdot^\circ\text{F})$ (kW/K)
CAV	= constant air volume
C_g	= fluid capacity rate of gas side, $\text{Btu}/(\text{hr}\cdot^\circ\text{F})$ (kW/K)
C_p	= specific heat capacity at constant pressure, $\text{Btu}/(\text{lbm}\cdot^\circ\text{F})$ ($\text{kJ}/(\text{kg}\cdot\text{K})$)
e	= error between $SAT_{lab,meas}$ and $SAT_{mfr,meas}$, $^\circ\text{F}$ ($^\circ\text{C}$)
DACC	= discharge (supply) air control of cooling
DACH	= discharge (supply) air control of heating

DOE	= Department of Energy
EAT	= exhaust air temperature, $^\circ\text{F}$ ($^\circ\text{C}$)
e_{cal}	= offset error for calibration of the manufactured-installed supply air temperature sensor, $^\circ\text{F}$ ($^\circ\text{C}$)
e_H	= error between $SAT_{th,pred}$ and $SAT_{mfr,meas}$, $^\circ\text{F}$ ($^\circ\text{C}$)
e_{eva}	= error between $SAT_{mfr,cal}$ and $SAT_{exp,eva}$, $^\circ\text{F}$ ($^\circ\text{C}$)
Hstage	= gas heating stage
\dot{m}	= mass flow rate, lb/hr (kg/s)
MAT	= mixed air temperature, $^\circ\text{F}$ ($^\circ\text{C}$)
MSAT	= measured manufacturer-installed supply air temperature
NTU	= number of transfer units
OADst	= outside air damper position
OAT	= outside air temperature, $^\circ\text{F}$ ($^\circ\text{C}$)
\dot{Q}_H	= gas heating capacity, Btu/hr (kW)
$Q_{loss,C}$	= heat loss in the supply air duct in cooling mode, Btu/hr (kW)
$Q_{loss,H}$	= heat loss in the supply air duct in heating mode, Btu/hr (kW)
r	= outside fresh air ratio
RTU	= rooftop air conditioning unit
RAT	= return air temperature, $^\circ\text{F}$ ($^\circ\text{C}$)
SAT	= supply air temperature, $^\circ\text{F}$ ($^\circ\text{C}$)
$SAT_{exp,eva}$	= indirect experimentally calculated true value of SAT, $^\circ\text{F}$ ($^\circ\text{C}$)
$SAT_{G,C}$	= measured SAT of the measuring grid in cooling mode, $^\circ\text{F}$ ($^\circ\text{C}$)
$SAT_{G,H}$	= measured SAT of the measuring grid in heating mode, $^\circ\text{F}$ ($^\circ\text{C}$)
$SAT_{lab,meas}$	= measured SAT with lab-installed temperature sensor, $^\circ\text{F}$ ($^\circ\text{C}$)
$SAT_{mfr,cal}$	= calibrated SAT for the manufacturer-installed temperature sensor, $^\circ\text{F}$ ($^\circ\text{C}$)
$SAT_{mfr,meas}$	= measured SAT with manufacturer-installed temperature sensor, $^\circ\text{F}$ ($^\circ\text{C}$)
$SAT_{O,C}$	= measured SAT at the outlet of supply air duct in cooling mode, $^\circ\text{F}$ ($^\circ\text{C}$)
$SAT_{O,H}$	= measured SAT at the outlet of supply air duct in heating mode, $^\circ\text{F}$ ($^\circ\text{C}$)
$SAT_{O,lab}$	= measured SAT with lab-installed sensor at the outlet of supply air duct, $^\circ\text{F}$ ($^\circ\text{C}$)
$SAT_{th,pred}$	= predicted theoretical true value of SAT, $^\circ\text{F}$ ($^\circ\text{C}$)
U	= heat transfer coefficient, $\text{Btu}/(\text{hr}\cdot^\circ\text{F}\cdot\text{ft}^2)$ ($\text{kW}/(\text{m}^2\cdot\text{K})$)
\dot{V}_C	= calculated supply air flow rate, cfm (m^3/s)

\dot{V}_{meas}	= measured supply air flow rate, cfm (m ³ /s)
ΔT_{fan}	= temperature rise across the supply fan, °F (°C)
v	= specific volume of air, ft ³ /lbm (m ³ /kg)
VAV	= variable air volume
ε	= heat exchanger effectiveness
ρ_a	= air density, lb/ft ³ (kg/m ³)

Subscripts

a	= air
C	= cooling
cal	= calibration
d	= design
eva	= evaluation
exp	= experimental
fan	= supply air fan
g	= gas
G	= grid
H	= heating
I	= inlet
lab	= lab-installed
$loss$	= heat loss
max	= maximum
$meas$	= measured
mfr	= manufacturer
min	= minimum
o	= outlet
O	= outlet of supply air duct
P	= constant pressure
$pred$	= predicted
th	= theoretical
ven	= ventilation

References

- ASHRAE. 2007. *ASHRAE Standard 62.1-2007, Ventilation for Acceptable Indoor Air Quality*. Atlanta, GA: American Society of Heating, Refrigerating and Air-conditioning Engineers, Inc.
- ASHRAE. 2009. *2009 ASHRAE Handbook—Fundamentals*. Atlanta, GA: American Society of Heating, Refrigerating and Air-Conditioning Engineers, Inc.
- ASME. 1974. *ANSI/ASME Standard PTC 19.3-1974 (R1998), Temperature measurement instruments and apparatus*. New York: American Society of Mechanical Engineers.
- Breuker, M.S. 1997. Evaluation of a statistical, rule-based fault detection and diagnostics method for vapor compression air conditioners. Master's thesis, School of Mechanical Engineering, Purdue University, West Lafayette, Indiana.
- Breuker, M.S., and J.E. Braun. 1998a. Common faults and their impacts for rooftop air conditioners. *International Journal of Heating, Ventilating, Air Conditioning and Refrigerating Research* 4(3):303–18.
- Breuker, M.S., and J.E. Braun. 1998b. Evaluating the performance of a fault detection and diagnostic system for vapor compression equipment. *International Journal of Heating, Ventilating, Air Conditioning and Refrigerating Research* 4(4):401–25.
- Katipamula, S., and M.R. Brambley. 2005. Methods for fault detection, diagnostics, and prognostics for building systems—a review, Part I. *HVAR&R Research* 11(1):3–25.
- Lennox. 2007. M1-7 Version 5.02 integrated modular controller (IMC). Dallas, TX: Lennox Technical Publication.
- Li, H., and J.E. Braun. 2003. An improved method for fault detection and diagnosis applied to packaged air conditioners. *ASHRAE Transactions* 109(2):683–92.
- Li, H., and J.E. Braun. 2007a. A methodology for diagnosing multiple-simultaneous faults in vapor compression air conditioners. *HVAS&R Research*, 13(2):369–95.
- Li, H., and J.E. Braun. 2007b. Decoupling features and virtual sensors for diagnosis of faults in vapor compression air conditioners. *International Journal of Refrigeration* 30(3):546–64.
- Li, H., and J.E. Braun. 2007c. An overall performance index for characterizing the economic impact of faults in direct expansion cooling equipment. *International Journal of Refrigeration* 30(2):299–310.
- Parmelee, G.V., and R.G. Huebscher. 1946. The shielding of thermocouples from the effects of radiation. *ASHRAE Transactions* 52:183.
- Rossi, T.M. 1995. Detection, diagnosis, and evaluation of faults in vapor compression cycle equipment. Ph.D. thesis, School of Mechanical Engineering, Purdue University, West Lafayette, Indiana.
- Rossi, T.M., and J.E. Braun. 1997. A statistical, rule-based fault detection and diagnostic method for vapor compression air conditioners. *International Journal of Heating, Ventilating, Air Conditioning and Refrigerating Research* 3(1):19–37.
- Westphalen, D., and S. Koszalinski. 2001. Energy consumption characteristics of commercial building HVAC systems: Volume I—chillers, refrigerant compressors, and heating systems. Final Report to the U.S. Department of Energy, Washington, DC (Contract No. DE-AC01-96CE23798).
- Wichman, A., and J.E. Braun. 2009. A smart mixed-air temperature sensor. *HVAR&R Research* 15(1):101–15.
- Yang, M., and H. Li. 2011. A virtual outside air ratio in packaged air conditioners. *HVAC&R Research* (forthcoming).

Appendix

Part A—experiment configuration

Sixteen heating experiments for assessment of direct measurements and indirect calculations of the SAT are performed in a lab with two artificial climate chambers. For evaluation purposes, an additional eight experiments in the cooling mode are also carried out.

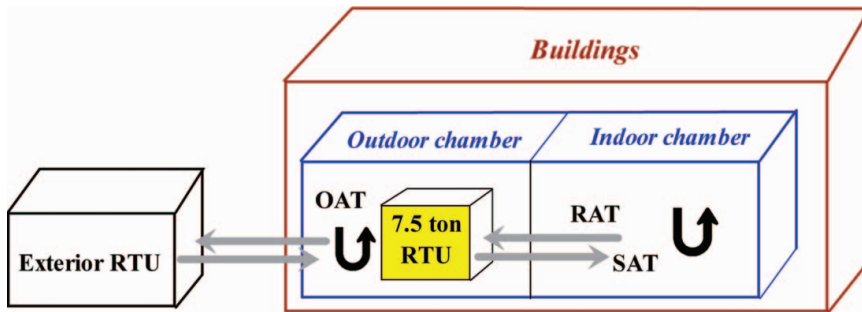


Figure 7. Illustration of machine layout in the lab.

System description

A 7.5-ton RTU equipped with two constant-speed compressors and a two-stage gas furnace with a 130,000 Btu/hr (38.1 kW) heating capacity composes the main experiment body (Figure 7). It sits in the outdoor environmental chamber and controls the indoor chamber with conditioned air. The nominal supply air flow rate is 2400 cfm (1.13m³/s) with a standard speed option. Together with another RTU outside of the building, artificial indoor and outdoor air physical conditions can be created and maintained.

Measurements description

Besides the MSAT sensor, there are more than ten additional important air temperature sensors as well as supportive temperature definitions. The measurements and concepts indispensable to accomplish the study are listed in what follows.

OAT

Since the manufacturer-installed OAT sensor is fixed beside the evaporator coils, improper heat gain and poor air distribution may affect the accuracy of the OAT measurements. Instead, a lab-installed OAT sensor mounted on the RTU outside the air inlet is used. The sensor, as are all other physical temperature sensors installed, has been calibrated with a precision of $\pm 0.5^\circ\text{F}$ (0.3°C).

Measurement of lab-installed SAT sensor

One more SAT sensor is installed in the RTU to supplement the measurement of SAT. The sensor is referred to as the lab-installed SAT sensor ($SAT_{lab,meas}$). The function is to verify and also backup the MSAT sensor in case of failure.

Supply fan temperature rise

ΔT_{fan} is calculated using the heat loss from the fan and is checked with actual measurements us-

ing the method presented by Wichman and Braun (2009) under conditions where neither mechanical cooling nor heating is operating.

The result of ΔT_{fan} in this article is 1.7°F (0.9°C) with an uncertainty of $\pm 0.2^\circ\text{F}$ (0.1°C). Since it is a CAV RTU, the uncertainty of the fan temperature rise is relatively small.

MAT

Accurate direct MAT measurements are notoriously difficult to obtain in RTUs due to space constraints and the use of small chambers for mixing outdoor and return air (ASME 1974). Much research has been conducted to indirectly obtain the accurate MAT measurements in RTUs. For example, Wichman and Braun (2009) proposed a smart MAT sensor for packaged systems that self-corrects the errors and accurately estimates the MAT using only a single-point measurement of MAT by correlating the errors with damper position signals and the temperature difference between outdoor and return air. Extensive lab testing demonstrates that the smart MAT sensor performs very well, and the overall root-mean-squared error is 0.57°F (0.3°C).

However, a physical MAT sensor is not typically installed in light commercial RTUs due to its bad performance, so this smart MAT sensor cannot be implemented without adding a new MAT sensor. To further simplify this technique, Yang and Li (2010) proposed an alternative method that eliminates the need of a physical MAT sensor and instead constructs a virtual MAT sensor to estimate MAT using damper position signals, OAT, RAT, and a calibrated virtual outdoor air ratio sensor. Both laboratory and field testing demonstrate an acceptable uncertainty of $\pm 1.0^\circ\text{F}$ (0.6°C). Since there is no pre-installed physical MAT sensor available in this study, the latter method was adopted.

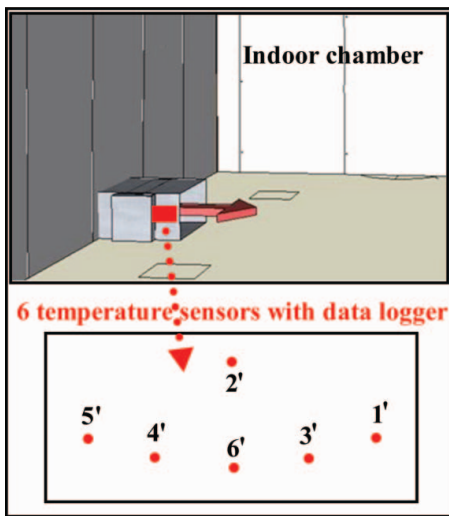


Figure 8. Sensors layout of additional six air temperature sensors.

Supply air flow rate

An air flow rate meter offering $\pm 1\%$ full-scale accuracy is mounted in the supply air duct in the lab. It has been calibrated and verified by using another flow hood.

Measurements of the measuring grid sensors

As presented previously, Figure 1 illustrates the arrangement of the measuring-grid temperature sensors. Eight sensors are symmetrically mounted at the supply air duct inlet.

Measurements of additional six air temperature sensors

Figure 8 depicts the installation of six air temperature sensors at the supply air duct outlet to the

indoor chamber. Measurements under both the cooling ($SAT_{O,C}$) and the heating ($SAT_{O,H}$) modes of these six air temperature sensors are collected.

Measurement of lab-installed temperature sensor at the supply air duct outlet

The sensor is referred to as a lab-installed temperature sensor at the supply air duct outlet ($SAT_{O,lab}$). The function is to verify the additional six temperature sensors at the supply air duct outlet in Figure 8.

Experiment settings

Experiment setups are collected in Table 6. To cover most combinations, both cooling and heating modes are conducted with different running stages, OADst, and OAT. The OAT is kept low for the heating mode and high for the cooling mode with reasonable distribution.

Each experiment assigned a scenario ID is conducted around 20 min for preparation, and followed by 10 to 15 min under steady status (Li and Braun 2003). Instant readings for each sensor are sampled every 15 s, and the mean of the samples is then used to represent the corresponding measurement result.

Part B—evaluation of $SAT_{O,C}$ and $SAT_{O,H}$

In the lab environment, the supply air duct is about 3.5 m long, connecting the outdoor chamber and the indoor chamber. In order to carry out the verification for this virtual calibration method, measurements of air temperature at the supply air duct outlet with six sensors are evaluated under both cooling and heating modes (Figure 9).

Table 6. Lab experiment settings.

Running mode	Running stage	OADst	OAT (°F (°C))	Scenario ID	Running mode	Running stage	OADst	OAT (°F (°C))	Scenario ID
Heating	2	0%	36.0 (2.2)	H-1	Heating	1	0%	35.6 (2.0)	H-9
Heating	2	0%	42.9 (6.1)	H-2	Heating	1	0%	45.9 (7.7)	H-10
Heating	2	0%	44.1 (6.7)	H-3	Heating	1	0%	44.4 (6.9)	H-11
Heating	2	0%	50.0 (10.0)	H-4	Heating	1	0%	49.2 (9.6)	H-12
Heating	2	30%	34.4 (1.3)	H-5	Heating	1	30%	34.1 (1.2)	H-13
Heating	2	30%	44.3 (6.8)	H-6	Heating	1	30%	42.9 (6.1)	H-14
Heating	2	30%	43.3 (6.3)	H-7	Heating	1	30%	43.1 (6.2)	H-15
Heating	2	30%	49.1 (9.5)	H-8	Heating	1	30%	48.4 (9.1)	H-16
Cooling	2	0%	81.8 (27.7)	C-1	Cooling	1	0%	79.6 (26.4)	C-5
Cooling	2	0%	87.8 (31.0)	C-2	Cooling	1	0%	81.8 (27.7)	C-6
Cooling	2	30%	82.3 (27.9)	C-3	Cooling	1	30%	81.9 (27.7)	C-7
Cooling	2	30%	87.0 (30.6)	C-4	Cooling	1	30%	86.4 (30.2)	C-8

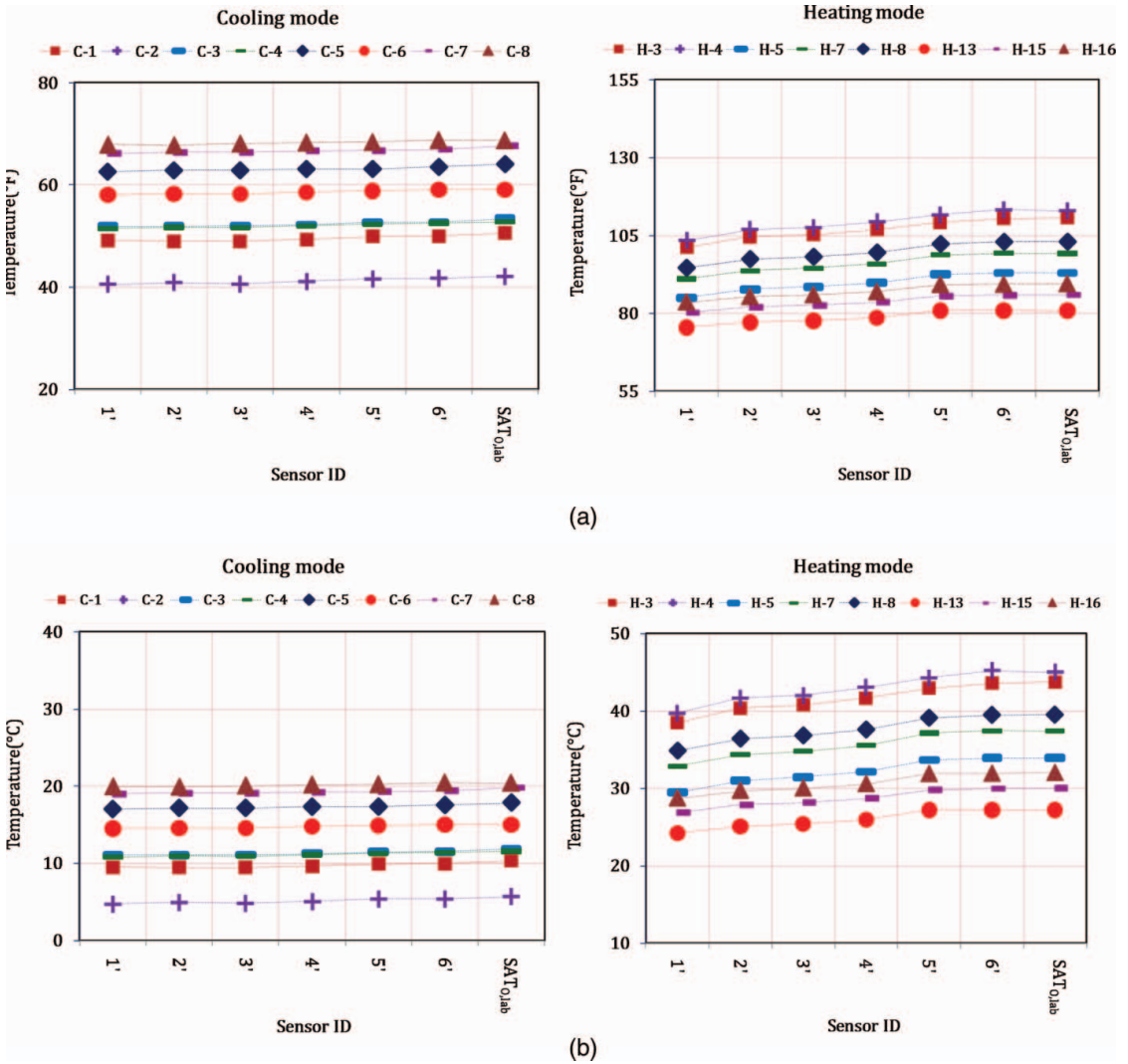


Figure 9. Evaluation of additional six temperature sensors under both cooling and heating modes: (a) IP units and (b) SI units.

Measurements of another lab-installed sensor at the supply air duct outlet ($SAT_{O,lab}$) are gathered for reference.

In the cooling mode, the average error between $SAT_{O,lab}$ and the mean of six $SAT_{O,C}$ is less than 1°F (0.6°C). In the meantime, in the heating mode, the error between $SAT_{O,lab}$ and the mean of six $SAT_{O,C}$ is lower 3°F (1.7°C). As expected, at the cross-section close to the outlet, air is well mixed and temperature distribution is fairly balanced. So in this study, the mean of six $SAT_{O,C}$ and the mean of six $SAT_{O,H}$ are used in the verification process.

Part C—uncertainty analysis of heating capacity

Referring to *ASHRAE Handbook—Fundamental* (ASHRAE 2009; Chapter 4), for heat exchangers), to calculate the heating transfer rate, mean temperature difference analysis and number of transfer units (NTU)-effectiveness (ϵ) analysis are used. The former method involves trial-and-error calculations, unless inlet and outlet fluid temperatures are known for both fluids. The NTU- ϵ method is adopted in the study.

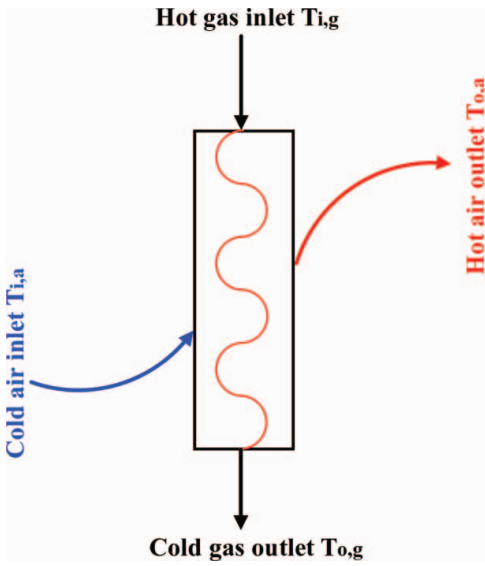


Figure 10. Heat transfer of heat exchanger.

Figure 10 shows the configuration of a counter-flow heat exchanger. $T_{i,a}$ and $T_{o,a}$ are the air temperature at the inlet and outlet of heat exchanger, respectively. $T_{i,g}$ and $T_{o,g}$ are the gas temperatures of the inlet and outlet of the heat exchanger. The maximum possible heat transfer rate $\dot{Q}_{H,max}$ occurs when the hot fluid enters at $T_{i,g}$ and leaves at the entering temperature of the cold fluid $T_{i,a}$:

$$\dot{Q}_{H,max} = C_{min} \times (T_{i,g} - T_{i,a}), \quad (14)$$

where $C_{min} = \min(C_g, C_a)$, $C_{max} = \max(C_g, C_a)$, wherein $C_g [(\dot{m} \times C_p)_g]$ and $C_a [(\dot{m} \times C_p)_a]$ are fluid capacity rates (Btu/(hr.°F), kW/K).

The actual heating capacity \dot{Q}_H can be calculated as

$$\dot{Q}_H = \dot{Q}_{H,max} \times \varepsilon. \quad (15)$$

The following three steps are needed in order to analyze the heating capacity and its uncertainty of a heat exchanger. Data from the 7.5-ton RTU are adopted for illustration purposes.

Step 1: calculation of C_r

According to the NTU- ε method, in a counter-flow heater, ε is determined by

$$\varepsilon = \frac{1 - \exp[-NTU(1 - C_r)]}{1 - C_r \times \exp[-NTU(1 - C_r)]} \quad (C_r < 1), \quad (16)$$

where $C_r = C_{min}/C_{max}$ as a capacity ratio.

To calculate C_r , the knowns and assumptions are listed below:

- the design heat exchanger effectiveness is $\varepsilon_d = 80\%$;
- the density and specific heat of air are $\rho_a = 0.07 \text{ lb/ft}^3$ (1.2 kg/m^3), $C_{p,a} = 0.24 \text{ Btu/(lbm}\cdot\text{°F)}$ ($1.005 \text{ kJ/(kg}\cdot\text{K)}$);
- the inlet temperature of air and natural gas are assumed as $T_{i,a} = 55.0^\circ\text{F}$ (12.8°C), $T_{i,g} = 3578^\circ\text{F}$ (1970°C);
- the design heating capacity and airflow rate are: $\dot{Q}_{H,d} = 130,000 \text{ Btu/hr}$ (38.1 kW), $\dot{V}_{a,d} = 144,000 \text{ ft}^3/\text{hr}$ (2400 cfm , $1.13 \text{ m}^3/\text{s}$).

If it is assumed that $C_g < C_a$, then according to the C_{min} and C_{max} definition, C_{min} equals C_g and C_{max} equals C_a :

- (1) $C_{min} = C_g$. The value of C_g can be obtained as Equation 17:

$$C_g = \frac{\dot{Q}_{H,d}}{(T_{i,g} - T_{i,a}) \times \varepsilon_d}. \quad (17)$$

In this case, C_g is $46.13 \text{ Btu/(hr}\cdot\text{°F)}$ (0.024 kW/K) as calculated.

- (2) $C_{max} = C_a$. With design airflow rate known, C_a can be derived from Equation 18:

$$C_a = \rho_a \times C_{p,a} \times \dot{V}_{a,d}. \quad (18)$$

The result is $C_a = 2419 \text{ Btu/(hr}\cdot\text{°F)}$ (1.423 kW/K).

Since C_a is significantly greater than C_g , the assumption holds for wide range airflow rate, giving

$$C_r = \frac{C_{min}}{C_{max}} = \frac{C_g}{C_a}. \quad (19)$$

And here it gives $C_r = 0.019$ for the design condition.

Step 2: correlating NTU

With $C_r = 0.019$ and $\varepsilon_d = 80\%$ at the design condition, from Equation 16, $NTU = 1.625$.

Step 3: uncertainty analysis of \dot{Q}_H

Combining Equations 15–19, for different operations, \dot{Q}_H can be expressed as Equation 20:

$$\dot{Q}_H = \frac{\dot{Q}_{H,d}}{\varepsilon_d} \times \varepsilon = \frac{\dot{Q}_{H,d}}{\varepsilon_d} \times \frac{1 - \exp\left[-NTU\left(1 - \frac{C_g}{C_a}\right)\right]}{1 - \frac{C_g}{C_a} \times \exp\left[-NTU\left(1 - \frac{C_g}{C_a}\right)\right]}$$

Where NTU is an intermediate variable derived from the variables of air side flow rate \dot{V}_a and gas-heated side flow rate \dot{V}_g , as shown in Table 7.

Therefore, fundamentally, uncertainty of heating capacity calculation is conducted with the indepen-

dent variables of V_a and V_g . The root sum square is used as Equation 21:

$$\delta \dot{Q}_H = \left[\left(\frac{\partial \dot{Q}_H}{\partial \dot{V}_a} \delta \dot{V}_a \right)^2 + \left(\frac{\partial \dot{Q}_H}{\partial \dot{V}_g} \delta \dot{V}_g \right)^2 \right]^{1/2}, \quad (21)$$

where $\delta \dot{V}_a$ and $\delta \dot{V}_g$ are uncertainties.

$\delta \dot{V}_a$ is $\pm 10\%$, which covers most conditions in the real operations (e.g., fouling). $\delta \dot{V}_g$ has a low value as $\pm 1\%$ because the natural gas regulator holds a high accuracy of pressure control. Consequently, it is found that uncertainty of heating capacity is only about $\pm 2\%$. Heating capacity is very stable and can be treated as a constant by just referring to the manufacturers' design values.

Table 7. Calculation of NTU and uncertainty analysis of heating capacity.

Equations (ASHRAE 2009)		
NTU	UA, C_{\min}	$h_a \leftarrow Nu_a \leftarrow Re_a \leftarrow V_a \leftarrow \dot{V}_a;$ $h_g \leftarrow Nu_g \leftarrow Re_g \leftarrow V_g \leftarrow \dot{V}_g$
$NTU = UA/C_{\min}$ Equation 22	$\left\{ \begin{aligned} \frac{1}{UA} &= \frac{1}{h_a A_a} + \frac{li(D_a/D_g)}{2\pi kL} + \frac{1}{h_g A_g} \\ &\text{Equation 23} \\ C_{\min} &= \text{Minimum}(C_a, C_g) \end{aligned} \right.$	$\left\{ \begin{aligned} h_a &= \frac{k_a}{D_a} Nu_a && \text{Equation 24} \\ Nu_a &= 0.3 + \frac{0.62 Re_a^{1/2} Pr_a^{1/3}}{[1+0.4/Pr_a]^{1/4}} [1 + (\frac{Re_a}{282,000})^{1/2}]^{1/4} && \text{Equation 25} \\ &(10,000 < Re_a < 40,000) \\ Re_a &= V_a D_a / \nu_a && \text{Equation 26} \\ V_a &= \dot{V}_a / A_a && \text{Equation 27} \\ h_g &= \frac{k_g}{D_g} Nu_g && \text{Equation 28} \\ Nu_g &= 0.023 Re_g^{4/5} Pr_g^{0.4} (Re_g > 10,000) && \text{Equation 29} \\ Re_g &= \rho V_g D_g / \mu_g && \text{Equation 30} \\ V_g &= \dot{V}_g / A_g && \text{Equation 31} \end{aligned} \right.$
Symbols		
A = area (ft ² (m ²)) C = heat air capacity rate ((Btu/(hr·°F), kW/K)) D = duct diameter (in. (m)) h = heat transfer coefficient (Btu/h·ft ² ·°F (kW/(m ² ·K))) k = thermal conductivity (Btu/h·ft·°F (kW/(m·K))) L = duct length (ft (m)) NTU = number of transfer units Nu = Nusselt number	Pr = Prandtl number Re = duct Reynolds number U = heat transfer coefficient ((Btu/(hr·°F·ft ²), kW/(m ² ·K))) ν = kinematic viscosity (ft ² /s (m ² /s)) V = linear velocity (ft/s (m/s)) \dot{V} = flow rate (ft ³ /s (m ³ /s)) ρ = density (lbm/ft ³ (kg/m ³)) μ = absolute viscosity (lbm/ft·s ((N·s)/m ²))	
Uncertainty analysis of heating capacity		
Independent variables	Input	Uncertainty
Flow rate of air side, \dot{V}_a , ft ³ /hr (m ³ /s)	144,000 (1.13)	±10%
Flow rate of gas heated air side, \dot{V}_g , ft ³ /hr (m ³ /s)	16,020 (0.13)	±1%
Dependent variable	Output	Uncertainty
Heating capacity, \dot{Q}_H (Btu/hr (kW))	130,000 (38.1)	±2%